HHS Public Access

Author manuscript

J Mol Biol. Author manuscript; available in PMC 2016 April 09.

Published in final edited form as:

J Mol Biol. 2016 March 27; 428(6): 1130–1141. doi:10.1016/j.jmb.2016.01.023.

Dlx5 homedomain/DNA complex; Structure, binding and effect of mutations related to split-hand and foot malformation syndrome

Andrew Proudfoot[1,2], **Herbert L. Axelrod**[1,3], **Michael Geralt**[1,2], **Robert J Fletterick**[4], **Fumiaki Yumoto**[4,#], **Ashley M. Deacon**[1,3], **Marc-André Elsliger**[1,2], **Ian A. Wilson**[1,2], **Kurt Wüthrich**[1,2,5,6], and **Pedro Serrano**[1,2,*]

[1]Joint Center for Structural Genomics (http://www.jcsg.org) [2]Department of Integrative Structural and Computational Biology, The Scripps Research Institute, 10550 North Torrey Pines Road, La Jolla, CA 92037, USA [3]Stanford Synchrotron Radiation Lightsource, SLAC National Accelerator Laboratory, Menlo Park, California 94025 USA [4]Department of Biochemistry and Biophysics, University of California San Francisco, 600 16th Street, San Francisco, CA 94158, USA [5]Skaggs Institute for Chemical Biology, The Scripps Research Institute, 10550 North Torrey Pines Road, La Jolla, CA 92037, USA. [6]Institute of Molecular Biology and Biophysics, ETH Zürich, CH-8093 Zürich, Switzerland

SUMMARY

The Dlx5 homeodomain is a transcription factor related to the Drosophila *Distal-less* gene that is associated with breast and lung cancer, lymphoma, Rett syndrome and osteoporosis in humans. Mutations in the DLX5 gene have been linked to deficiencies in craniofacial and limb development in higher eukaryotes, including Split Hand and Foot Malformation-1 (SHFM-1) in humans. Our characterization of a Dlx5 homeodomain–$(CGACTAATTAGTCG)_2$ complex by NMR spectroscopy paved the way for determination of its crystal structure at 1.85 Å resolution that enabled rationalization of the effects of disease-related mutations on the protein function. A remarkably subtle mutation, Q186H, is linked to SHFM-1; this change likely affects affinity of DNA binding by disrupting water-mediated interactions with the DNA major groove. A more subtle effect is implicated for the Q178P mutation, which is not in direct contact with the DNA. Our data indicate that these mutations diminish the ability of the Dlx5 homeodomain to recognize and bind target DNAs, and likely destabilize the formation of functional complexes.

[*]*Correspondence* (serrano@scripps.edu).

[#]*Current address:* Structural Biology Research Center, KEK/High Energy Accelerator Research Organization, Tsukuba, Ibaraki 305-0801, Japan

AUTHOR CONTRIBUTIONS

AP, AMD, MAE, IAW, KW and PS conceived and designed the experiments. RJF and FY provided de DNA template from which the Dlx5 homeodomain was cloned. AP and PS designed and analyzed the biophysical experiments. AP produced the samples for all structural and biophysical experiments with assistance from MG, and AP, KW and PS performed and analyzed NMR experiments. HAL performed crystal structure determination and analysis. AP, HAL, MAE, IAW, KW and PS wrote the manuscript.

INTRODUCTION

DLX5 is one of six vertebrate genes related to the *Distal-less* (D*ll*) gene of *Drosophila* [1, 2]. It plays a key role in craniofacial and limb development as well as in sensory organ morphogenesis [3, 4]. DLX5 also promotes tumor cell proliferation in lymphomas and lung cancers by binding to the promoter region of *MYC*, which is a proto-oncogene that encodes a DNA binding factor and regulates transcription and cell cycle progression in many human cancers [5]. *DLX* genes encode homeodomain transcription factors that are primarily expressed during early embryogenesis [2] and regulate intercellular signaling across the interface between the neural and non-neural ectoderm, which is critical for inducing and patterning adjacent cell fates [6]. *DLX5* is expressed in the median plane of the Apical Ectodermal Ridge (AER), which is essential for the establishment of the correct limb polarity and its development in the proximo-distal direction, along with the formation of digits [7, 8]. In humans, the six *DLX* genes are linked and convergently transcribed as gene pairs (*DLX1* and *DLX2*, *DLX5* and *DLX6*, and *DLX3* and *DLX7*) that share regulatory elements and expression patterns [9, 10]. In mice, *DLX5* and *DLX6* are expressed in a unique spatial and temporal pattern; they are first detected in embryos at the 8.5 – 9 day stage and appear in the developing forebrain by day 10. Between days 12 and 15, the gene products are expressed in brain and developing bones and, by day 17, their levels start to slowly decrease [11].

In mice, both *DLX5* and *DLX6* need to be simultaneously inactivated for generation of an abnormal phenotype that leads to split limb malformation and defective development of the middle portion of the AER as well as axial skeletal and inner ear defects [12]. However, in humans, mutation or inhibition of *DLX5* alone is linked to Split Hand and Foot Malformation-1 (SHFM-1) [4].

SHFM, also known as ectrodactyly, is characterized by the absence of one or more of the central rays of the autopod along with varying degrees of fusion of the remaining digits. The phenotype can vary between affected family members or even between different limbs of the affected individual, and can range from mild syndactyly of three or four fingers, to severe ‘lobster claw’ like hands or feet [13, 14]. SHFM affects approximately 1 in 18,000 newborns [15] and can occur by itself or as part of a more complex syndrome with abnormalities in other parts of the body [13, 16–21].

The most common form of SHFM in humans, SHFM-1, was mapped to a 1.5 Mb chromosomal region encoding *DLX5*, *DLX6*, and *DSS1* [21, 22], all of which participate in the Wnt signaling pathway, which plays an important role in limb development [4]. Two independent reports, each concerning two affected individuals, have linked missense mutations in the *DLX5* gene resulting in the amino-acid substitutions Q178P and Q186H to the onset of SHFM-1. While Q178P and Q186H segregate in an autosomal recessive and dominant fashion, respectively [8, 23], both lead to reduced transcriptional activity [8]. While *DLX5* had previously been suggested to be involved with the onset of SHFM-1, these were the first reported cases of linking affected individuals to mutations in the *DLX5* gene.

Due to the limited long-term stability of free Dlx5, structural studies of the homeodomain required an engineered variant containing a fusion with GB1, a protein which is often used as a solubility tag in NMR studies of proteins prone to aggregation or precipitation. NMR spectroscopy could then be used as an analytical tool to monitor protein stability, to search for a dsDNA sequence amenable for the production of diffracting crystals, and to study the formation of the complex in solution. Dlx5 in complex with the dsDNA sequence CGACTAATTAGTCG showed improved stability, which allowed the removal of the Gb1 tag from the DNA complex prior to screening of crystallization conditions. The Dlx5–$(CGACTAATTAGTCG)_2$ structure was then determined by X-ray crystallography at 1.85 Å resolution, and revealed that the residues associated with SHFM-1 were involved in key interactions for DNA recognition and binding. The effect of these mutations on thermal stability and binding affinity was further evaluated using circular dichroism (CD) spectroscopy and isothermal titration calorimetry (ITC). Our results indicate that the onset of SHFM-1 is likely linked to obstacles in the formation of functional Dlx5:DNA complexes.

RESULTS

NMR study of the interactions between the Dlx5 homeodomain and DNA duplexes

The Dlx5 construct used for NMR studies includes the entire homeodomain (residues 137–198), which has limited long-term stability and was therefore not amenable for screening of DNA partners. To overcome these limitations, the Dlx5 homeodomain was cloned into a vector containing an N-terminal Gb1 solubility tag linked via a TEV-protease cleavage site to the homeodomain. Gbx1-Dlx5 remained soluble during purification. NMR spectroscopy had a key role in monitoring Gbx1-Dlx5 and Dlx5 stability, in confirming that the globular structure was preserved during the different purification steps, and for the search of a suitable partner dsDNA (See Materials and Methods). For example, we observed that after TEV cleavage of a freshly purified sample, Dlx5 was stable for a few hours and could be used to acquire NMR spectra for the study of interactions with DNA (Fig. 1). We also observed that once a complex with DNA was formed, Dlx5 was more stable and that we could cleave GB1 from the DNA-bound Dlx5 before starting crystallization trials. A 21 bp DNA sequence, AAATGCAGCCA**TAAT**TAGAGT, had previously been identified to target expression of the Dlx5/Dlx6 bi-gene cluster to the developing forebrain in mice [24]. This sequence includes the **TAAT** motif typically recognized by homeodomains, including all six Dlx proteins [25]. For NMR studies, GC nucleotide pairs were added to the 5’ and 3’ ends of the 21-bp DNA to enhance stability (25 bp dsDNA, *GG*AAATGCAGCCA**TAAT**TAGAGT*CG*). The 2D [^{15}N-^{1}H]-HSQC spectrum was recorded in the presence of 1.5 equivalents of the 25 bp DNA and only exhibited 51% of the expected HN signals (data not shown), which indicated that this fragment was not optimal for structural studies. Subsequently, based on reported crystal structures determined in the presence of shorter DNA sequences such as 2H1K (15-bp), 3CMY (14-bp), 1NK2 (16-bp), 9ANT (15-bp), a 14 bp DNA fragment, CGAC**TAAT**TAGTCG, containing the key TAAT binding element was evaluated. 2D [^{15}N,^{1}H]-HSQC spectra of Dlx5 were recorded in the presence of 0.0, 0.5, 1.0 and 1.5 equivalents of the 14-bp DNA (Figure 1). All expected peaks were observed in the Dlx5 NMR spectrum, but at a substoichiometric concentrations of DNA, several peaks broadened and disappeared, presumably due to intermediate rate

exchange in the NMR time scale between the free and bound protein (Figure 1B). Upon saturation of Dlx5 with the 14-bp DNA, all 70 expected backbone amide resonances of the protein were again observed (Figure 1, C and D), which indicated a one to one protein:DNA ratio in the complex. This is consistent with the elution profile of the Dlx5-GB1:DNA complex from a Hi-Load 26/60 Superdex 75 gel filtration column (Figure 2A). A peak with absorbance at both 280 and 260 nm eluted from the column at 181 ml, corresponding to a species of approximately 25 kDa, in agreement with the expected size of the Dlx5-GB1:DNA complex. This peak was analyzed by SDS PAGE and agarose gel electrophoresis(Figure 2, B and C) to confirm the presence of both protein and DNA in the sample.

Crystal structure of Dlx5 in complex with DNA

Overview of the Structure—The crystal structure of the human Dlx5 homeodomain in complex with the palindromic 14-bp CGACTAATTAGTCG DNA duplex was determined by molecular replacement at a resolution of 1.85 Å in a triclinic (P1) space group (Figure 3A). The Matthews' coefficient was 3.1 $Å^3$/Dalton, with an estimated solvent content of 65 %. A summary of the data collection, modeling and refinement statistics is provided in Table 1. The crystallographic asymmetric unit (ASU) contained two Dlx5-DNA complexes and 232 water molecules. The polypeptide backbone atoms of the two protein molecules in the ASU can be superimposed with an RMSD of 0.31 Å, and the Ramachandran plot produced by MolProbity showed that 100 % of the residues are in favored regions. Analysis of the content of the ASU with the EBI-PISA server did not identify any potentially stable quaternary assembly. Size exclusion chromatography further supported this result, since the predominant state in solution corresponds to one protein bound to one DNA duplex. The expressed protein consists of 65 residues (137–198), which represent the entire homeodomain of Dlx5, plus four N-terminal residues (GHMV) that remained after cleavage of the purification/solubility tag. This tetrapeptide segment and the first 3 residues of the homeodomain were disordered in both protein molecules (chains A and D) in the ASU and consequently were not included in the structure. Additional regions not included in the model due to lack of electron density, include V137 and the side-chain atoms of R154 and K193 in molecule A and V137, K194, and N198 in molecule D. The bound DNA molecules (BC and EF) consist of a 14-bp palindromic DNA duplex (5'-CGACTAATTAGTCG-3') were all clearly visible in the electron density with the exception of one nucleotide at the 3' end of DNA (identified as strand F in the coordinate file).

The structure of Dlx5 consists of three α-helices and includes the typical homeodomain 'helix-turn-helix' motif [26]. Residues 146–159 form α-helix 1 and lie parallel to α-helix 2 of residues 164–174. α-helix 3 (residues 178–197) is aligned roughly perpendicular to α-helix 2 and inserts into the major groove of the DNA duplex. It is worth noting that despite the palindromic nature of the dsDNA sequence, which could suggest the existence of multiple binding sites, the presence of a single major groove ensures the formation of a one to one Dlx5:dsDNA complex. The DNA adopts a B-form architecture with standard Watson-Crick base pairing observed throughout the duplex, except at one end where bases 1 and 14 interact with bases from the DNA duplex of a symmetry-related molecule, forming a triple

helix-type interaction similar to that observed in the Msx-1 homeodomain/DNA complex crystal structure [27].

DNA- Recognition and Binding—The high structural similarity between Dlx5:dsDNA and multiple homeodomain:DNA complexes in the Protein Data Bank (PDB) provided a strong foundation for comparisons of the effect of amino acid substitutions on complex formation. Homologous to what has been observed in other homeodomain:DNA complexes, the majority of short-range protein-DNA contacts involve nucleotides on the major grove and residues on α-helix 3 of Dlx5, specially the side chains of N187, R189, and K191. Examination of structures of other PF000476 homeodomain Pfam family members indicates that the N187 side chain, which is within hydrogen bonding distance of the base of Ade 7, makes a key interaction with DNA, since it is observed in all members of the family. The functional importance of N187 is also supported by the fact that a His mutation at the equivalent positions in human Hox-13 is linked to hand-foot genital syndrome [28], as a result of a strong reduction of binding affinity of NANOG to DNA [29].

In addition to the direct hydrogen-bonding interaction with DNA, our structure indicates that the side chain of N187, along with the conserved Q186, is part of an extended water-mediated interaction network with DNA (Figures 3B and 4). Although Q186 is positioned too far from the DNA for direct hydrogen bonding, a conserved water molecule bridges its side-chain amide with that of N187. This water molecule is also within hydrogen bonding distance of the Thy7 nucleotide base. R189 and K191 are also functionally important and play key roles in DNA binding along the major groove by forming salt-bridges with the DNA phosphate groups. Mutation of R189 in the human HESX-1 homeobox protein is linked to septooptic dysplasia, and Axenfeld-Rieger syndrome is related to a homologous mutation in human PIX2 [30]. Additional interactions with the major groove are mediated by Y161, which is located on loop connecting α-helices 1 and 2. The Y161 aromatic side chain is stacked against the side chain of R189, forming a cation-π interaction, which anchors the positions of both side chains for binding the phosphate group of Cyt4.

Whereas the binding interface at the major groove primarily involves residues of α-helix 3 of the Dlx5 homeodomain, the interface at the minor groove is formed from residues on the N-terminal arm of the protein [31]. The R138 sidechain interacts with Thy9 and the backbone amide of K139. The highly conserved R141 contacts Thy9, and a natural variant mutation at the structurally equivalent site on the human homeobox protein aristaless-like 4 has been linked to parietal foramina [32]. Recognition of the DNA minor grove also involves hydrogen-bond interactions mediated by T142, as well as non-polar contacts between P140 and Ade7.

Study of the effect of SHFM-1 linked mutations on protein stability and DNA binding

The effect of the Q178P and Q186H amino acid replacements on protein and protein:DNA complex stability was analyzed using CD spectroscopy. The thermal denaturation profile of the wild type (WT) Dlx5 homeodomain is shown in Figure 5 and compared to that of the Dlx5[Q178P] and Dlx5[Q186H] homeodomains in the absence and presence of bound DNA. The denaturation curves are sigmoidal and indicate that all regular secondary structures

disappear at 80 °C. The unfolding mid-point for the WT Dlx5 and Dlx5[Q178P] mutant are 54.3 and 54.7 °C, respectively, while a lower unfolding temperature of 52.6 °C was observed for Dlx5[Q186H]. Upon complex formation, a ~5 °C increase in thermal stability was observed for the WT and Dlx5[Q178P] homeodomains, but only a ~1 °C increase for Dlx5[Q186H].

The effects of the Q178P and Q186H mutations on the binding of the 14-bp DNA were further investigated using isothermal titration calorimetry (ITC) (Figure 6). Binding of the Dlx5 homeodomain to DNA is exothermic and could be fit to a single-site binding model. All variants show a single transition and the stoichiometry parameters (N) indicate that one protein molecule binds to one DNA duplex. WT Dlx5 binds to the 14-bp DNA with high affinity (K_d = 0.16 ± 0.02 μM), which is driven by a favorable change of enthalpy (ΔH^o = −8.4 kcal mol^{-1}). Titrations performed with the variant proteins show that both amino-acid substitutions reduce the binding affinity, with two-fold (K_d = 0.33 ± 0.04 μM) and a ten-fold (K_d = 1.8 ± 0.12 μM) reductions for Dlx5[Q178P] and Dlx5[Q186H], respectively. This five-fold difference in binding activity contrasts with the results from transcriptional activity experiments that revealed that both mutations lead to a similar reduction of *MYC* expression in HEK293 and HeLa cells.

DISCUSSION

Dlx5 is a homeodomain transcription factor that is expressed in the developing brain and bones of higher eukaryotes during early embryogenesis. The protein plays a key role in craniofacial, and limb development and is involved with regulation of the *MYC* promoter, which is implicated with many human cancers. Interaction of various DNA molecules with the Dlx5 homeodomain were evaluated by NMR, including a 14 bp palindromic DNA duplex (CGACTAATTAGTCG), which had been used in previous homeodomain:DNA binding studies in our laboratory (unpublished data). Analysis of [^{15}N-^{1}H]-HSQC spectra of the Dlx5 homeodomain in the presence and absence of this 14 bp DNA showed that addition of equimolar amounts of DNA induced large changes in the chemical shifts of multiple backbone amide resonance signals, indicating that complex formation had occurred (Figure 1). In addition, the NMR profile [33] of Dlx5 in the presence this DNA duplex showed that all expected peaks were present in the spectrum with homogeneous intensities. Together, these results indicated that a Dlx5-homeodomain–DNA complex was indeed formed and that any exchange between the free and DNA-bound forms of the protein was occurring on an intermediate NMR chemical shift time scale [34]. Guided by these NMR studies, the crystal structure of Dlx5 in complex with the 14 bp DNA was determined at 1.85 Å resolution and exhibits a typical homeodomain:DNA structure (Otting et al., 1990), in which helix α3 occupies the major grove and the N-terminal end contacts the minor grove (Figure 3).

Point mutations in the DLX*5* gene (Q178P and Q186H) have been identified in individuals affected with SHFM-1, a congenital limb-development disorder affecting the central rays of the autopod [8, 23]. Q186 is located in the middle of helix α3 of the homeodomain structure within the protein-DNA binding interface (Figure 3C). Q186, which corresponds to Q50 in standard homeodomain nomenclature [35], is preserved in all six Dlx proteins and highly conserved in other homeodomains. Only a few residues types can be tolerated in position 50

and, while glutamine is most common, some homeodomain structures contain lysine, serine or cysteine instead [36]. Q50 and N51 play important roles in DNA binding specificity and affinity through a series of coordinated water mediated interactions [37, 38]. In Dlx5, mutation of Q186 to histidine decreases binding affinity and protein stability, both in the presence and absence of DNA. This effect is most likely due to the disruption of water-mediated interactions involving Q186 and N187 of the homedomain, and Ade6, Ade7 and Thy8 of the DNA (Figure 4). The second mutation linked to SHFM-1 involves residue Q178, which is preserved across all six Dlx homeodomains and is highly conserved within DLX5 genes from different species [23]. Q178 corresponds to Q42 in the standard homeodomain nomenclature, and is positioned too far from the DNA and is typically occupied by a glutamic acid involved in a salt bridge with R167 (R31), which is one of three highly conserved salt bridges that are believed to play a role in stabilizing the homeodomain structure [35]. Mutations of residues in positions 31/42 induce stabilizing or destabilizing effects on the protein. These mutations also play a role in altering the affinity of the homeodomain for its respective DNA sequences. In the Dlx5 homeodomain, Q178P mutation has no significant effect on the thermal stability in the presence or absence of DNA, which suggests that Q178/R167 interactions are not important for protein stability. The Q178P mutation does however result in a two-fold reduction in affinity of the Dlx5 homeodomain for the 14 bp DNA. Analysis of the Dlx5:DNA structure suggests that, although Q178 does not directly contact DNA (Figure 3C), it seems to help position R167 for proper contact with the phosphate backbone of the DNA, either directly or mediated via a water molecule (Fig. 4). The Q178P mutant lacks this positioning effect, which results in a small reduction in affinity for DNA binding.

The crystal structure in combination with the CD and ITC measurements has therefore helped to rationalize the effects of the Q178P and Q186H mutations that are linked to SHFM-1. Both mutations reduce the affinity of the Dlx5 homeodomain for target DNAs, but their mechanisms of action are different. Whereas the Q186H mutant directly impacts the recognition of the major grove, Q178P acts in a subtler way, by preventing the neighboring R167 attaining the appropriate conformation and orientation to form a salt bridge with phosphate groups in the DNA. The contrast between the different effect of the two mutations on DNA binding affinity and their similar impact on the expression of *MYC* [8], suggests that these amino acid substitutions disturb the behavior of Dlx5 at multiple functional levels.

EXPERIMENTAL PROCEDURES

Cloning of the Dlx5 Homeodomain

Residues 137 to 198 were amplified from a *H. sapiens* Dlx5 construct and cloned into pET28Gb1TeV, which is a pET28b plasmid modified in-house to contain a Gb1 solubility tag and TEV cleavage site between the NcoI and NdeI restriction site. The primers used for PCR were: Primer A: 5’ cccCATATGgttcgtaaacccaggactatttattcc 3’ and Primer B: 5’ gggagAAGCTTttagtttttcatgatcttcttgatcttg 3’. Primer A contains an NdeI restriction site (capitalized) and the first 27 nucleotides of the Dlx5 homeodomain. Primer B contains the last 26 nucleotides of the Dlx5 homeodomain, a stop codon, and a Hind III restriction site (capitalized). Mutagenesis of residues 178 and 186 was performed using QuickChange site-

directed mutagenesis (Stratagene) and the following primers: Primer 178: 5' cctcgctgggattgacaccaacacaggtgaaaatctgg 3' and Primer 186: 5' cacaggtgaaaatctggtttcacaacaaaagatccaag 3'. The nucleotides mutated form wild-type are in bold typeface and underlined.

Protein Production

Dlx5 variants were expressed in *E. coli* strain BL21(DE3) (Novagen) grown in M9 medium containing D-glucose (4 g/L) and $^{15}NH_4Cl$ (1 g/L) as the sole carbon and nitrogen sources respectively. Cell cultures were grown at 37 °C with vigorous shaking to an optical density of 0.6 at 600 nm, and the temperature then reduced to 18 °C before Dlx5 expression was induced with 1 mM isopropyl-β-D-1-thiogalactopyranoside. The cells were then grown at 18 °C for 20 hours and harvested by centrifugation (10,000 × g for 5 minutes). The harvested cells were re-suspended in buffer A (20 mM sodium phosphate at pH 7.4, 200 mM sodium chloride, 20 mM imidazole), supplemented with Complete EDTA-free protease inhibitor cocktail tablets (Roche), and lysed by sonication. Cell debris was removed by centrifugation (40,000×g for 30 minutes) and the supernatant was loaded onto a Ni^{2+} affinity column (HisTrap HP; GE Healthcare) equilibrated with buffer A. The imidazole concentration was increased to 50 mM to remove non-specific proteins and then to 500 mM to elute Dlx5. Fractions identified to contain Dlx5, as determined by SDS-PAGE, were digested for 1 hour with 0.08 mg/ml TEV protease at room temperature. The digested protein was loaded onto an SP sepharose AC IEX column (GE Healthcare) equilibrated with buffer B (20 mM sodium phosphate pH 6.0, 50 mM sodium chloride) and the protein eluted with 1 M sodium chloride gradient over 20 column volumes. Fractions containing Dlx5 were pooled and further purified using a Superdex™ 75 HiLoad™ 26/60 (GE Healthcare) size exclusion chromatography column equilibrated in buffer B. Fractions containing Dlx5 were concentrated to a final protein concentration of 1.2 mM using a 3 kDa cut-off centrifugal filter devices (Millipore). Dlx5 samples that were to be analyzed using NMR spectroscopy were supplemented with 5% ^2H_2O (v/v) and 4.5 mM sodium azide.

Preparation of DNA

Single-stranded DNA sequences, purchased from Invitrogen, were re-suspended with nano-pure water to a final concentration of 1 mM and equimolar concentrations of complimentary strands were combined. Using an Eppendorf Mastercycler gradient PCR machine, samples were heated to 95 °C for 5 minutes. The samples were then cooled every 2 minutes in 5 °C increments to a final temperature of 20 °C. As trace amounts of tri-ethyl amine were detected, double-stranded DNA was further purified using Illustra NAP-25 columns (GE Healthcare) and DNA was eluted using nano-pure water. DNA samples were lyophilized overnight and re-suspended in nano-pure water to a final concentration of 15 mM.

NMR Spectroscopy

1:1.1 Dlx5:DNA samples were prepared by addition of double-stranded DNA sequences to a 1 mM protein solution. The 2D [^{15}N, ^1H]-HSQC spectra used to study the Dlx5 – DNA interaction were recorded at 298K with 1024 × 256 complex data points, on a Bruker DRX 700 MHz spectrometer equipped with a 1.7-mm microcoil probehead.

Preparation of Dlx5:DNA Complex for Crystallography

Harvested cells were re-suspended in buffer A supplemented with Complete EDTA-free protease inhibitor cocktail tablets (Roche), lysed by sonication, and purified using Ni^{2+} affinity and ion exchange chromatography as detailed above. Fractions eluting from the SP sepharose column that were identified to contain Dlx5 were pooled and a 1.1 molar ratio of the DNA duplex CGAC**TAATTAG**TCG was added to the sample and left at room temperature for 1 hour. The Dlx5:DNA complex was further purified using a Superdex™ 75 HiLoad™ 26/60 (GE Healthcare) size exclusion chromatography column equilibrated in buffer C (20 mM MES pH 8.0, 50 mM sodium chloride). Fractions containing both protein and DNA as determined by SDS-PAGE, and agarose gel electrophoresis were combined and digested for 2 hours with 0.08 mg/ml TEV protease at room temperature, before being loaded onto a Ni^{2+} affinity column equilibrated in buffer C, to remove both the purification tag and the TEV protease. Fractions containing Dlx5:DNA complex were concentrated using a 3 kDa centrifugal filter device to a final protein concentration of 10 mg / ml.

Crystallization

The Dlx5:DNA complex was crystallized using the nanodroplet vapor diffusion method [39] with standard JCSG crystallization protocols [40, 41]. Sitting drops composed of 100 nl protein solution were mixed with 100 nl crystallization solution in a sitting drop format on our robotic JCSG Rigaku CrystalMation high-throughput system and equilibrated against a 50 µl reservoir at 289 K for 42 days prior to harvest. The crystallization reagent consisted of 0.08M sodium chloride, 45% 2-methyl-2,4-pentanediol, 0.012M spermine tetrahydrochloride, 0.1M sodium cacodylate pH 6.0. Additional 2-Methyl-2,4-pentanediol was added to a final concentration of 50% (v/v) as a cryoprotectant.

Data collection, structure determination, and refinement of the crystal structure

Initial screening for diffraction was carried out using the Stanford Automated Mounting system (SAM) [42] at the Stanford Synchrotron Radiation Lightsource (SSRL, Menlo Park, CA). X-ray diffraction data were collected at SSRL beam line 14-1 at 100 K using a Rayonix MX-325 CCD detector at a wavelength of 1.000 Å and indexed in the triclinic space group P1. All data were processed using the JCSG's distributed structure determination pipeline XSOLVE [43] that performed integration and scaling of the data using MOSFLM and XSCALE respectively [44]. Primary phasing was accomplished by molecular replacement using both the protein backbone and sidechain atoms of the Msx-1 homeodomain/DNA complex (PDB ID 1IG7), which has 59% sequence identity with DLX5, using PHASER [45], and refinement was carried out with REFMAC5 [46]. Initial positioning of the two protein molecules in the asymmetric unit following restrained refinement of the molecular replacement solution resulted in an elevated R_{cryst} of 46% and R_{free} of 48%, and poor electron density maps as the protein contributes only approximately 50% of the scattering material in the unit cell with DNA comprising the remainder. Therefore, the molecular replacement calculations were repeated using both the protein molecule and a portion of the DNA molecule from the Msx-1 Homeodomain/DNA complex (PDB ID 1IG7) in close-range interactions with the protein (residues 22 – 26 on the B chain of 1IG7 and residues 8 – 12 on the C-chain). The resulting structure yielded improved R-

values and electron density maps (R_{cryst}=37.5%, R_{free}=43.2%). ARP/wARP was used to re-build the protein model with the amino-acid sequence of the Dlx5 construct, and resulted in a model with 122 of the total 128 residues and an R_{cryst} of 33.5% and R_{free} of 37.1%. Model building was performed throughout using COOT [47]. The electron density maps were of sufficient quality to manually model the nucleotide sequence of the DNA fragment co-crystallized with the Dlx5 construct into the model, as well as water molecules. Further rounds of model building and TLS refinement yielded a model with an R_{cryst} of 18.3% and R_{free} of 22.5%. X-ray data collection and refinement statistics are compiled in Table 1.

Validation and deposition

The quality of the crystal structure was analyzed using the JCSG Quality Control server (see http://smb.slac.stanford.edu/jcsg/QC/). This server verifies: the stereo chemical quality of the model using AutoDepInputTool [48], MolProbity [49], and WHATIF 5.0 [50]; agreement between the atomic model and the data using SFcheck 4.0 [51], and RESOLVE [52]; the protein sequence using CLUSTALW [53]; atom occupancies using MOLEMAN2.0 [54]; and consistency of NCS pairs. It also evaluates differences in R_{cryst}/R_{free}, expected R_{free}/R_{cryst}, and maximum/minimum B-values by parsing the refinement log-file and header of the coordinates file. Protein quaternary structure analyses were performed using the EBI PISA server [55] and 2Fo-Fc omit electron density maps were calculated using PHENIX [56]. Figure 3 was prepared with PyMOL [57].

ITC Experiments

ITC was performed on a MicroCal™ Auto-ITC_{200} (GE Healthcare). All samples were extensively dialyzed into buffer C (20 mM sodium phosphate pH 6.0, 300 mM sodium chloride) to avoid any heat of dilution from mixing buffers. 100 μM protein solutions were titrated at a constant temperature of 25 °C, into a sample cell containing 7.5 μM 14 bp dsDNA sequence. Each titration consisted of a preliminary 0.5 μl injection followed by 24 injections of 1.6 μl. The protein and DNA concentrations were measured after dialysis using a NanoDrop® ND-1000 spectrophotometer by measuring the absorbance at 280 and 260 nm respectively. The raw calorimetry data were integrated and analyzed to obtain the binding constant, stoichiometry, and binding enthalpy along with the error margins, using the ITC data analysis package of the Origin software.

CD Experiments

20 μM protein or complex in buffer C was placed in a 0.1 cm path length quartz cuvette and CD experiments were recorded using the Temperature/Wavelength Scan software supplied with the Jasco 815 CD spectrophotometer. Unfolding profiles over the range 20 – 95 °C were measured at a constant wavelength of 209 nm and increasing the temperature at a rate of 1.0 °C/minute.

PDB accession numbers

The atomic coordinates of the Dlx5:DNA complex crystal structure have been deposited in the Protein Data Bank with accession code 4RDU.

Acknowledgments

This work was supported by the Joint Center for Structural Genomics (JCSG) through the NIH Protein Structure Initiative (PSI) grant U54 GM094586 from the National Institute of General Medical Sciences (www.nigms.nih.gov). Kurt Wüthrich is the Cecil H. and Ida M. Green Professor of Structural Biology at The Scripps Research Institute. We thank the members of the JCSG high-throughput structural biology pipeline for their contribution to this work. Portions of this research were carried out at the Stanford Synchrotron Radiation Lightsource, a Directorate of SLAC National Accelerator Laboratory and an Office of Science User Facility operated for the U.S. Department of Energy Office of Science by Stanford University. The SSRL Structural Molecular Biology Program is supported by the DOE Office of Biological and Environmental Research, and by the National Institutes of Health, National Institute of General Medical Sciences (including P41GM103393) and the National Center for Research Resources (P41RR001209). The contents of this publication are solely the responsibility of the authors and do not necessarily represent the official views of NIGMS, NCRR or NIH.

References

1. Cohen SM, Bronner G, Kuttner F, Jurgens G, Jackle H. Distal-less encodes a homeodomain protein required for limb development in Drosophila. Nature. 1989; 338:432–434. [PubMed: 2564639]
2. Merlo GR, Zerega B, Paleari L, Trombino S, Mantero S, Levi G. Multiple functions of Dlx genes. Int. J. Dev. Biol. 2000; 44:619–626. [PubMed: 11061425]
3. Ferrari D, Harrington A, Dealy CN, Kosher RA. Dlx5 in limb initiation in the chick embryo. Dev. Dyn. 1999; 216:10–15. [PubMed: 10474161]
4. van Silfhout AT, van den Akker PC, Dijkhuizen T, Verheij JBGM, Olderode-Berends MJW, Kok K, et al. Split hand/foot malformation due to chromosome 7q aberrations(SHFM1): additional support for functional haploinsufficiency as the causative mechanism. Eur. J. Hum. Genet. 2009; 17:1432–1438. [PubMed: 19401716]
5. Xu J, Testa JR. DLX5 (distal-less homeobox 5) promotes tumor cell proliferation by transcriptionally regulating MYC. J. Biol. Chem. 2009; 284:20593–20601. [PubMed: 19497851]
6. Elliott AM, Evans JA. Genotype-phenotype correlations in mapped split hand foot malformation (SHFM) patients. Am. J. Med. Genet A. 2006; 140A:1419–1427. [PubMed: 16688749]
7. Robert B. Bone morphogenetic protein signaling in limb outgrowth and patterning. Dev. Growth Diff. 2007; 49:455–468.
8. Wang X, Xin Q, Li L, Li J, Zhang C, Qiu R, et al. Exome sequencing reveals a heterozygous DLX5 mutation in a Chinese family with autosomal-dominant split-hand/foot malformation. Eur. J. Hum. Genet. 2014; 22:1105–1110. [PubMed: 24496061]
9. Depew MJ, Lufkin T, Rubenstein JLR. Specification of jaw subdivisions by Dlx genes. Science. 2002; 298:381–385. [PubMed: 12193642]
10. Wieland I, Muschke P, Jakubiczka S, Volleth M, Freigang B, Wieacker PF. Refinement of the deletion in 7q21.3 associated with split hand/foot malformation type 1 and Mondini dysplasia. J. Med. Genet. 2004; 41:e54. [PubMed: 15121782]
11. Simeone A, Acampora D, Pannese M, Desposito M, Stornaiuolo A, Gulisano M, et al. Cloning and characterization of two members of the vertebrate Dlx gene family. Proc. Nat. Acad. Sci. USA. 1994; 91:2250–2254. [PubMed: 7907794]
12. Merlo GR, Paleari L, Mantero S, Genova F, Beverdam A, Palmisano GL, et al. Mouse model of split hand/foot malformation type I. Genesis. 2002; 33:97–101. [PubMed: 12112878]
13. Duijf PHG, van Bokhoven H, Brunner HG. Pathogenesis of split-hand/split-foot malformation. Hum. Mol. Genet. 2003; 12:R51–R60. [PubMed: 12668597]
14. van Bokhoven H, Hamel BCJ, Bamshad M, Sangiorgi E, Gurrieri F, Duijf P PHG, et al. p63 gene mutations in EEC syndrome, limb-mammary syndrome, and isolated split hand-split foot malformation suggest a genotype-phenotype correlation. Am. J. Hum. Genet. 2001; 69:481–492. [PubMed: 11462173]
15. Elliott AM, Evans JA, Chudley AE. Split hand foot malformation (SHFM). Clin. Genet. 2005; 68:501–505. [PubMed: 16283879]

16. Boles RG, Pober BR, Gibson H, Willis CR, McGrath J, Roberts DJ, et al. Deletion of chromosome 2q24-q31 causes characteristic digital anomalies - Case-report and review. Am. J. Hum. Genet. 1995; 55:155–160.
17. de Mollerat XJ, Gurrieri F, Morgan CT, Sangiorgi E, Everman DB, Gaspari P, et al. A genomic rearrangement resulting in a tandem duplication is associated with split hand-split foot malformation 3 (SHFM3) at 10q24. Hum. Mol. Genet. 2003; 12:1959–1971. [PubMed: 12913067]
18. Faiyaz-Ul-Haque M, Zaidi SHE, King LM, Haque S, Patel M, Ahmad M, et al. Fine mapping of the X-linked split-hand/split-foot malformation (SHFM2) locus to a 5.1-Mb region on Xq26.3 and analysis of candidate genes. Clin. Genet. 2005; 67:93–97. [PubMed: 15617554]
19. Ianakiev P, Kilpatrick MW, Toudjarska I, Basel D, Beighton P, Tsipouras P. Split-hand/split-foot malformation is caused by mutations in the p63 gene on 3q27. Am. J. Hum. Genet. 2000; 67:59–66. [PubMed: 10839977]
20. Khan S, Basit S, Zimri FK, Ali N, Ali G, Ansar M, et al. A novel homozygous missense mutation in WNT10B in familial split-hand/foot malformation. Clin. Genetics. 2012; 82:48–55.
21. Scherer SW, Poorkaj P, Allen T, Kim J, Geshuri d, Nunes M, et al. Fine mapping of the autosomal-dominant split hand split foot locus on chromosome-7, band q21.3-q22.1. Am. J. Hum. Genet. 1994; 55:12–20. [PubMed: 8023840]
22. Crackower MA, Scherer SW, Rommens JM, Hui CC, Poorkaj P, Soder S, et al. Characterization of the split hand/split foot malformation locus SHFM1 at 7q21.3-q22.1 and analysis of a candidate gene for its expression during limb development. Hum. Mol. Genet. 1996; 5:571–579. [PubMed: 8733122]
23. Shamseldin HE, Faden MA, Alashram W, Alkuraya FS. Identification of a novel DLX5 mutation in a family with autosomal recessive split hand and foot malformation. J. Med. Genet. 2012; 49:16–20. [PubMed: 22121204]
24. Poitras L, Yu M, Lesage-Pelletier C, Macdonald RB, Gagne JP, Hatch G, et al. An SNP in an ultraconserved regulatory element affects Dlx5/Dlx6 regulation in the forebrain. Development. 2010; 137:3089–3097. [PubMed: 20702565]
25. Scott MP, Tamkun JW, Hartzell GW. The structure and function of the homeodomain. Biochim. Biophys. Acta. 1989; 989:25–48. [PubMed: 2568852]
26. Qian Y, Billeter M, Otting G, Muller M, Gehring W, Wüthrich K. The structure of the Antennapedia homeodomain determined by NMR spectroscopy in solution: comparison with prokaryotic repressors. Cell. 1989; 59:573–580. [PubMed: 2572329]
27. Hovde S, Abate-Shen C, Geiger JH. Crystal structure of the Msx-1 homeodomain/DNA complex. Biochemistry. 2001; 40:12013–12021. [PubMed: 11580277]
28. Goodman FR, Bacchelli C, Brady AF, Brueton LA, Fryns JP, Mortlock DP, et al. Novel HOXA13 mutations and the phenotypic spectrum of hand-foot-genital syndrome. Am. J. Hum. Genet. 2000; 67:197–202. [PubMed: 10839976]
29. Jauch R, Ng CKL, Saikatendu KS, Stevens RG, Kolatkar PR. Crystal structure and DNA binding of the homeodomain of the stem cell transcription factor Nanog. J. Mol. Biol. 2008; 376:758–770. [PubMed: 18177668]
30. Semina EV, Ferrell RE, Mintz-Hittner HA, Bitoun P, Alward WLM, Reiter RS, et al. A novel homeobox gene PITX3 is mutated in families with autosomal-dominant cataracts and ASMD. Nature Genet. 1998; 19:167–170. [PubMed: 9620774]
31. Otting G, Qian Y, Billeter M, Muller M, Affolter M, Gehring W, et al. Protein-DNA contacts in the structure of a homeodomain-DNA complex determined by nuclear magnetic resonance spectroscopy in solution. EMBO J. 1990; 9:3085–3092. [PubMed: 1976507]
32. Wuyts W, Cleiren E, Homfray T, Rasore-Quartino A, Vanhoenacker F, Van Hul W. The ALX4 homeobox gene is mutated in patients with ossification defects of the skull (foramina parietalia permagna, OMIM 168500). J. Med. Genet. 2000; 37:916–920. [PubMed: 11106354]
33. Pedrini B B, Serrano P, Mohanty B, Geralt M, Wüthrich K. NMR-profiles of protein solutions. Biopolymers. 2013; 99:825–831. [PubMed: 23839514]
34. Wüthrich, K. NMR of Proteins and Nucleic Acids. New York: Wiley; 1986.

35. Torrado M, Revuelta J, Gonzalez C, Corzana F, Bastida A, Asensio JL. Role of conserved salt bridges in homeodomain stability and DNA binding. J. Biol. Chem. 2009; 284:23765–23779. [PubMed: 19561080]
36. Duan JX, Nilsson L. The role of residue 50 and hydration water molecules in homeodomain DNA recognition. Eur. Biophy. J. Biophys Lett. 2002; 31:306–316.
37. Chi YI. Homeodomain revisited: a lesson from disease-causing mutations. Hum. Genet. 2005; 116:433–444. [PubMed: 15726414]
38. Grant RA, Rould MA, Klemm JD, Pabo CO. Exploring the role of glutamine 50 in the homeodomain-DNA interface: Crystal structure of engrailed (Gln50 ->Ala) complex at 2.0 angstrom. Biochemistry. 2000; 39:8187–8192. [PubMed: 10889025]
39. Santarsiero BD, Yegian DT, Lee CC, Spraggon G, Gu J, Scheibe D, et al. An approach to rapid protein crystallization using nanodroplets. J. Appl. Cryst. 2002; 35:278–281.
40. Lesley SA, Kuhn P, Godzik A, Deacon AM, Mathews I, Kreusch A, et al. Structural genomics of the Thermotoga maritima proteome implemented in a high-throughput structure determination pipeline. Proc. Nat. Acad. Sci. USA. 2002; 99:11664–11669. [PubMed: 12193646]
41. Elsliger MA, Deacon A, Godzik A, Lesley SA, Wooley J, Wüthrich K, et al. The JCSG high-throughput structural biology pipeline. Acta Crystallogr. Sect. F Struct. Biol. Cryst. Commun. 2010; 66:1137–1142.
42. Cohen AE, Ellis PJ, Miller MD, Deacon AM, Phizackerley RP. An automated system to mount cryo-cooled protein crystals on a synchrotron beamline, using compact sample cassettes and a small-scale robot. J. Appl. Crystallogr. 2002; 35:720–726. [PubMed: 24899734]
43. van den Bedem H, Wolf G, Xu Q, Deacon AM. Distributed structure determination at the JCSG. Acta Crystallogr D Biol Crystallogr. 2011; 67:368–375. [PubMed: 21460455]
44. Kabsch W. Automatic processing of rotation diffraction data from crystals of initially unknown symmetry and cell constants. J. Appl. Crystallogr. 1993; 26:795–800.
45. McCoy AJ. Solving structures of protein complexes by molecular replacement with Phaser. Acta Crystallogr. D Biol. Crystallogr. 2007; 63:32–41. [PubMed: 17164524]
46. Murshudov GN, Skubak P, Lebedev AA, Pannu NS, Steiner RA, Nicholls RA, et al. REFMAC5 for the refinement of macromolecular crystal structures. Acta Crystallogr. D Biol. Crystallogr. 2011; 67:355–367. [PubMed: 21460454]
47. Emsley P P, Cowtan K. Coot: model-building tools for molecular graphics. Acta Crystallogr. D Biol. Crystallogr. 2004; 60:2126–2132. [PubMed: 15572765]
48. Yang H, Guranovic V, Dutta S, Feng Z, Berman HM, Westbrook JD. Automated and accurate deposition of structures solved by X-ray diffraction to the Protein Data Bank. Acta Crystallogr. D Biol. Crystallogr. 2004; 60:1833–1839. [PubMed: 15388930]
49. Chen VB, Arendall WB 3rd, Headd JJ, Keedy DA, Immormino RM, Kapral GJ, et al. MolProbity: all-atom structure validation for macromolecular crystallography. Acta Crystallogr. D Biol. Crystallogr. 2010; 66:12–21. [PubMed: 20057044]
50. Vriend G. WHAT IF: a molecular modeling and drug design program. J. Mol. Graph. 1990; 52:52–56. [PubMed: 2268628]
51. Vaguine AA, Richelle J, Wodak SJ. SFCHECK: a unified set of procedures for evaluating the quality of macromolecular structure-factor data and their agreement with the atomic model. Acta Crystallogr. D Biol. Crystallogr. 1999; 55:191–205. [PubMed: 10089410]
52. Terwilliger T. SOLVE and RESOLVE: automated structure solution, density modification and model building. J. Synchrotron. Radiat. 2004; 11:49–52. [PubMed: 14646132]
53. Chenna R, Sugawara H, Koike T, Lopez R, Gibson TJ, Higgins DG, et al. Multiple sequence alignment with the Clustal series of programs. Nucleic Acids Res. 2003; 31:3497–3500. [PubMed: 12824352]
54. Kleywegt GJ. Validation of protein models from Calpha coordinates alone. J. Mol. Biol. 1997; 273:371–376. [PubMed: 9344745]
55. Krissinel E, Henrick K. Inference of macromolecular assemblies from crystalline state. J. Mol. Biol. 2007; 372:774–797. [PubMed: 17681537]

56. Adams PD, Afonine PV, Bunkoczi G, Chen VB, Davis IW, Echols N, et al. PHENIX: a comprehensive Python-based system for macromolecular structure solution. Acta Crystallogr. D Biol. Crystallogr. 2010; 66:213–221. [PubMed: 20124702]

57. Schrodinger L. The PyMOL Molecular Graphics System, Version 1.6.x. 2010

58. Luscombe NM, Laskowski RA, Thornton JM. NUCPLOT: a program to generate schematic diagrams of protein-nucleic acid interactions. Nucl. Acids Res. 1997; 25:4940–4945. [PubMed: 9396800]

59. Diederichs K, Karplus PA. Improved R-factors for diffraction data analysis in macromolecular crystallography. Nat. Struct.Biol. 1997; 4:269–275. [PubMed: 9095194]

60. Weiss MS, Metzner HJ, Hilgenfeld R. Two non-proline cis peptide bonds may be important for factor XIII function. FEBS Lett. 1998; 423:291–296. [PubMed: 9515726]

61. Weiss MS, Hilgenfeld R. On the use of the merging R factor as a quality indicator for X-ray data. J. Appl. Crystallogr. 1997; 30:203–205.

62. Cruickshank DW. Remarks about protein structure precision. Acta Crystallogr. D Biol. Crystallogr. 1999; 55:583–601. [PubMed: 10089455]

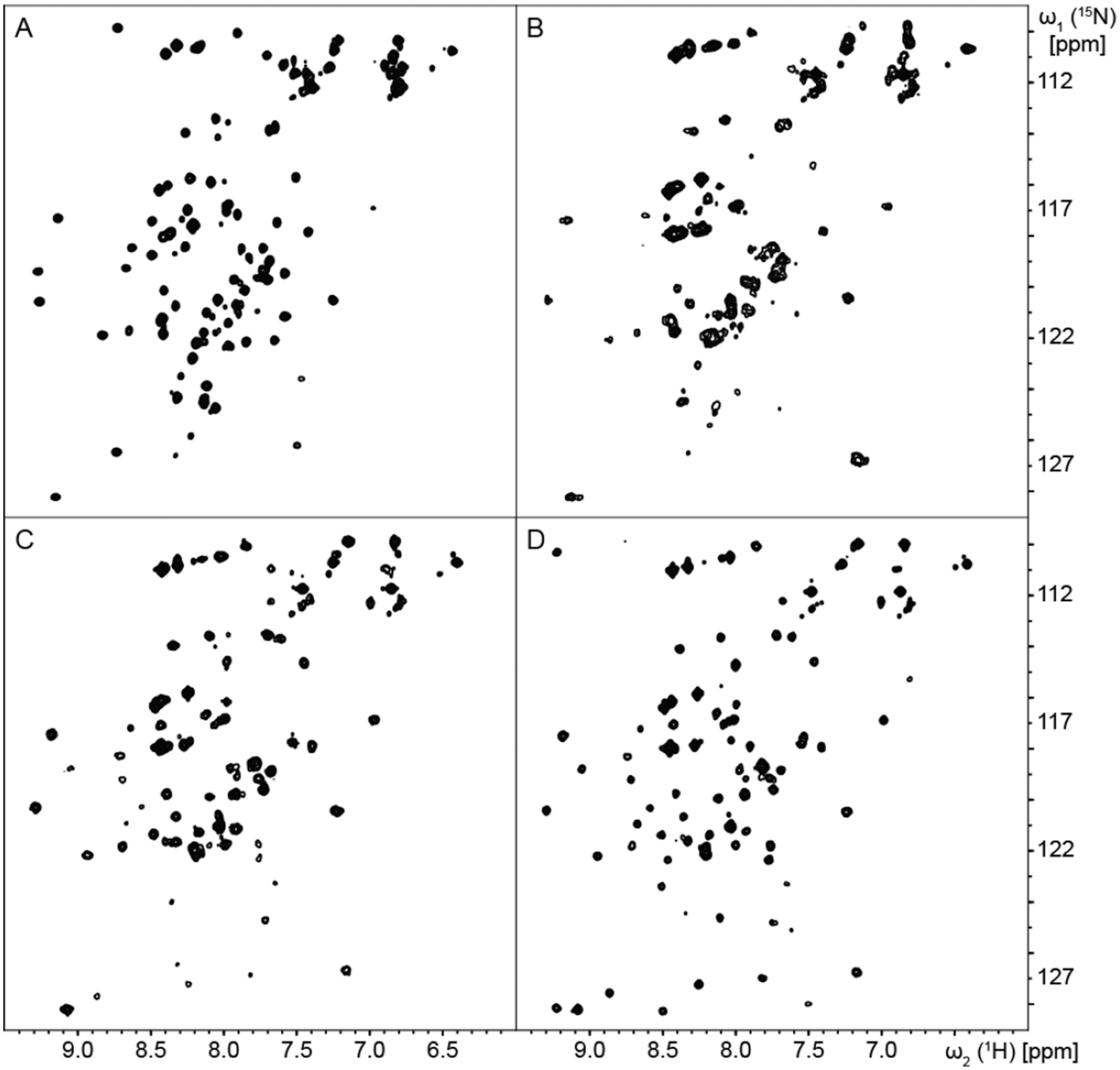

Figure 1. Binding of the Dlx5 homeodomain to the CGACTAATTAGTCG dsDNA as monitored by NMR

(A–D) Contour plots are shown of 2D [^{15}N, ^{1}H]-HSQC spectra of a 1.2 mM solution of ^{15}N-labelled Dlx1 containing variable amounts of DNA. (A) no DNA. (B) 0.6 mM. (C) 1.2 mM. (D) 1.8 mM. All spectra were recorded with Dlx5 prepared by TEV cleavage of freshly-purified GB1-Dlx5 fusion protein (see materials and methods).

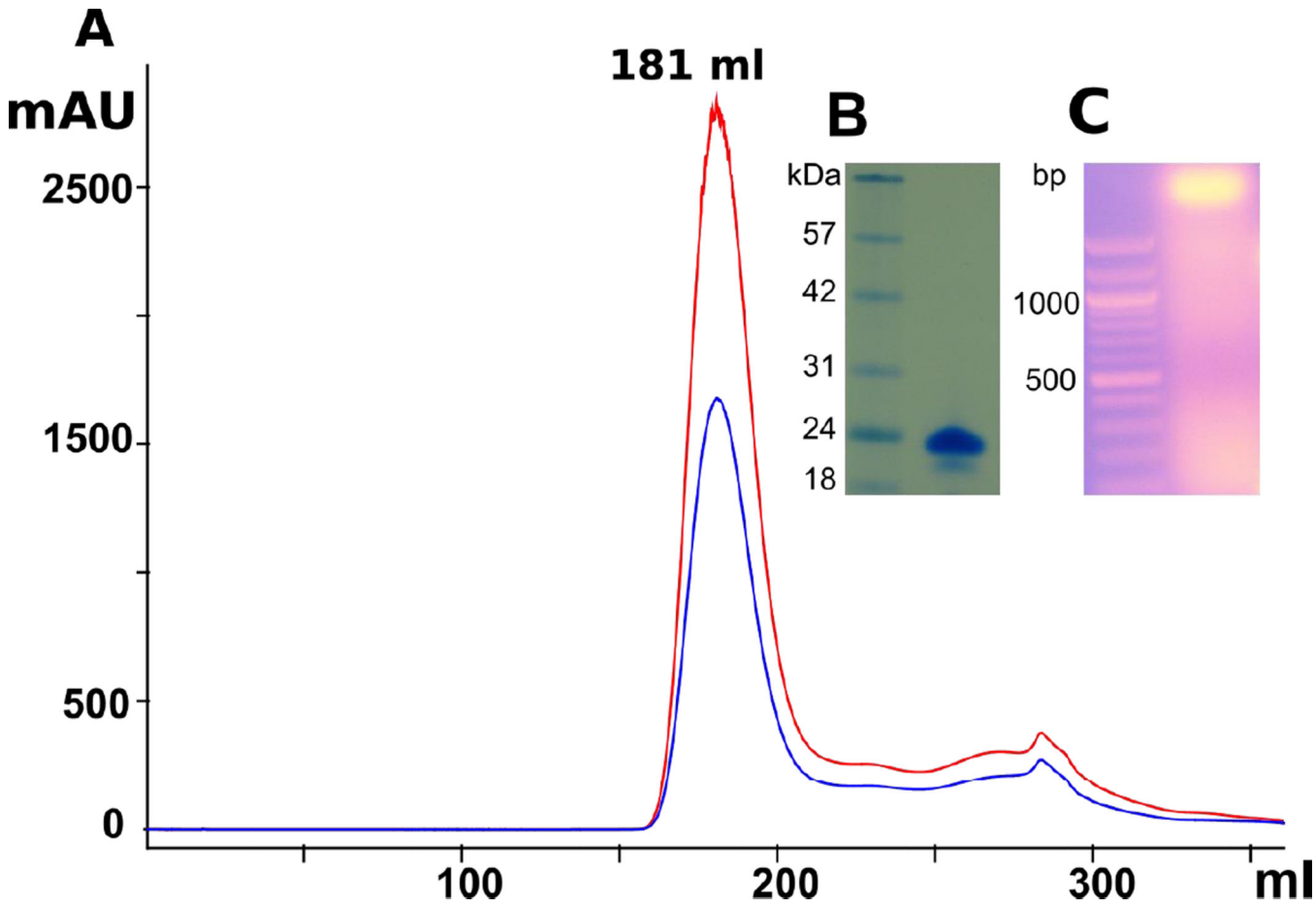

Figure 2. Purification of the Dlx5 homeodomain GB1 fusion protein:DNA complex

(A) Elution profile of the Dlx5-GB1:DNA complex from a HiLoad 26/60 Superdex 75 gel filtration column monitored at 260 nm (red) and 280 nm (blue). The inserts show further characterization of the sample eluted from the gel filtration column at 181 ml. (B) SDS PAGE. (C) Agarose gel electrophoresis. In (B) and (C), lane 1 contains BioPioneer AccuRuler RGB Broad Range protein marker and New England Biolabs 100 bp DNA ladder, respectively.

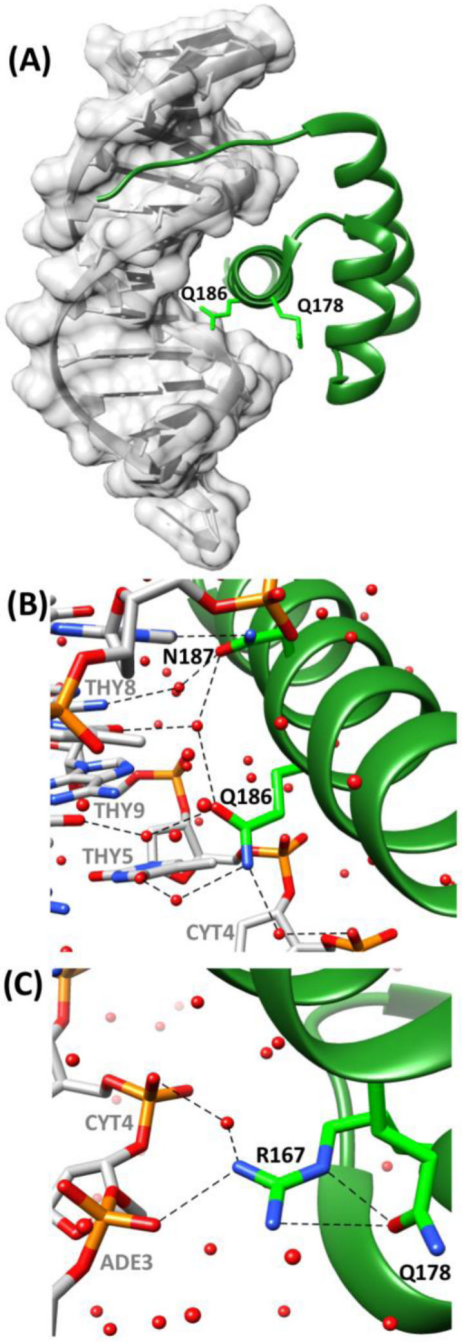

Figure 3. Crystal structure of the Dlx5 homeodomain in complex with the CGACTAATTAGTCG dsDNA

(A) Structure of the Dlx5 complex with CGACYAATTAGTCG. Dlx5 is shown in a dark green ribbon representation. The side chains of Q178 and Q186 are presented as sticks, with nitrogen and oxygen atoms colored blue and red, respectively. The dsDNA is shown in grey as a superposition of its van der Waals surface and ribbon representation of the backbone and side-chain atoms. (B) Close-up view of Q186 and N187 indicating direct and water-mediated interactions with dsDNA. Water molecules are shown as red spheres. N-O and O-O distance shorter than 3.0 Å are shown in black broken lines. Nitrogen, oxygen and

phosphorous atoms are colored blue, red and orange, respectively (C) Close-up view showing hydrogen-bond interactions between Q178, R167 and the dsDNA, using the same presentation as in (B).

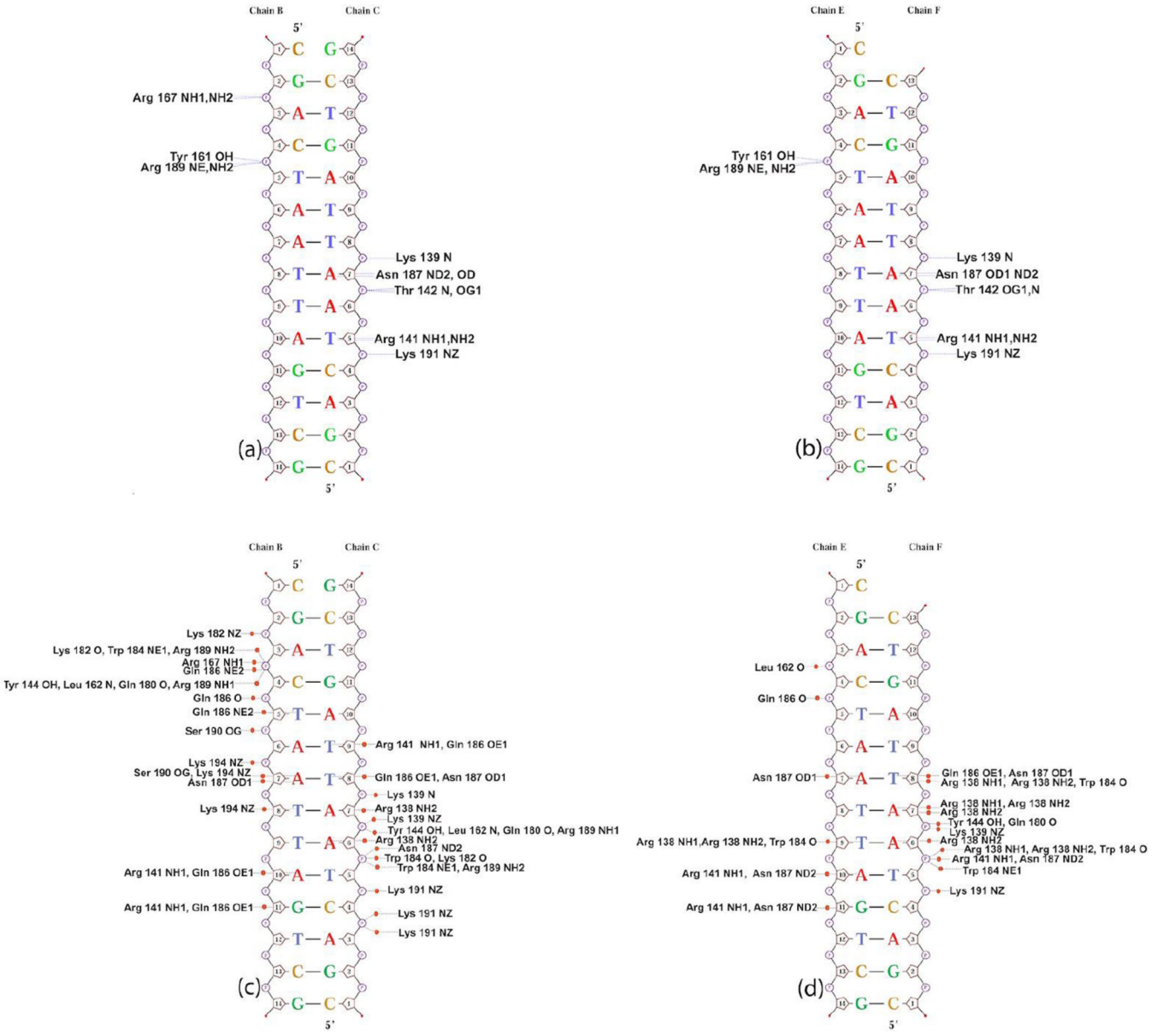

Figure 4. Schematic representation of hydrogen bonding and non-polar contacts (<3.5 Å) in the Dlx5 homeodomain-DNA complex

Nucplot was used [58]. Left and right panels show close range interactions of the two Dlx5:DNA complexes in the crystal asymmetric unit. One complex includes Dlx5 represented as a monomer A with its bound double-stranded DNA (B and C DNA strands as identified in the PDB file), while the other is formed by the second Dlx5 (monomer D) with bound double-stranded DNA (E and F strands). Asterisks denote residues that interact with more than one nucleotide.

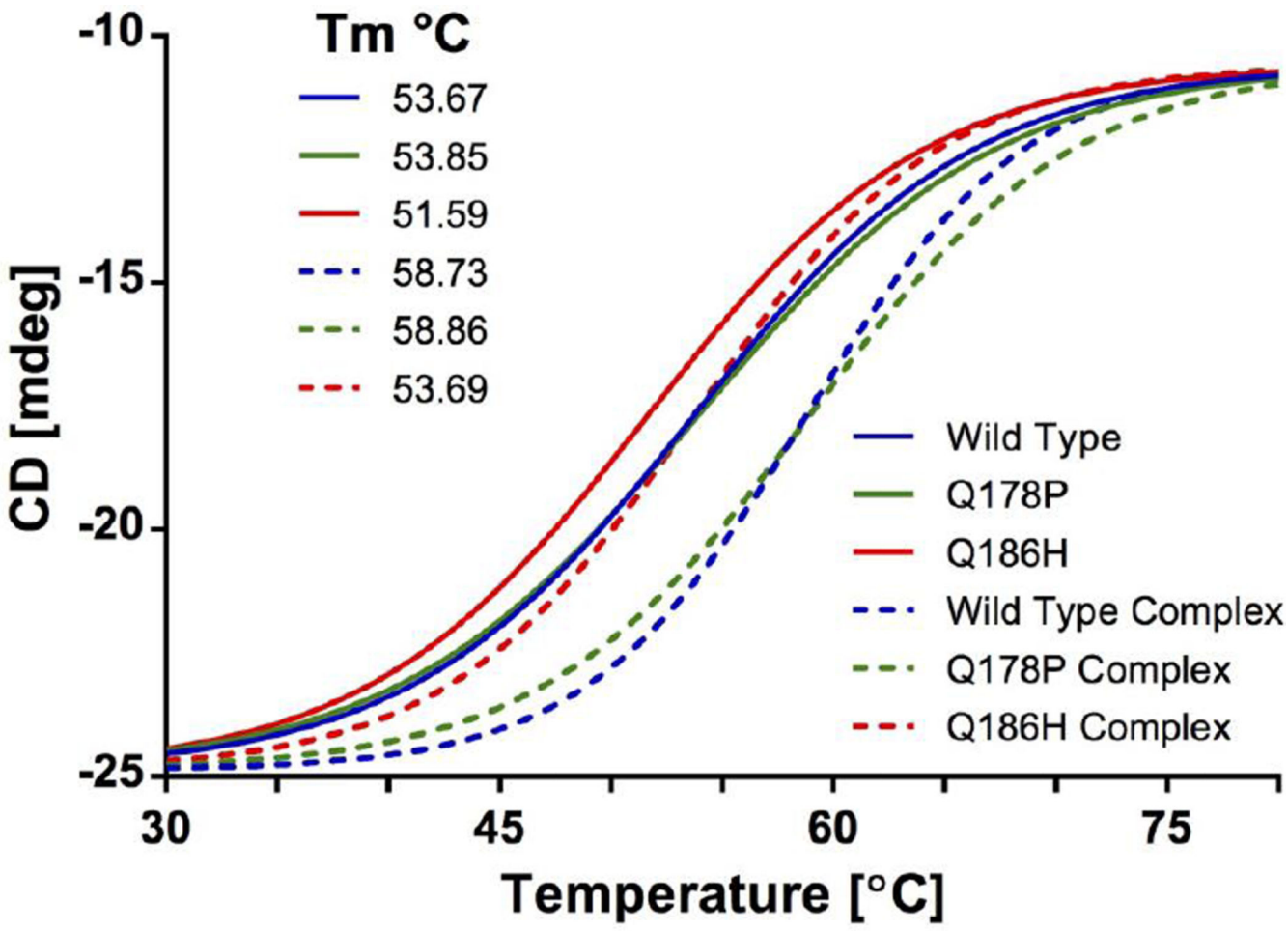

Figure 5. Temperature-induced denaturation of the Dlx5 and the variant Dlx5[Q178P] and Dlx5[Q186H] homeodomains

Solid and dashed lines represent CD measurements recorded in the presence and absence of equimolar concentrations of the CGACTAATTAGTCG dsDNA. The temperature variation of the signal intensity was monitored at 209 nm during heating over the range from 30 °C to 80 °C. Resulting profiles for Dlx5, Dlx5[Q178P] and Dlx5[186H] are shown in blue, green, and red, respectively.

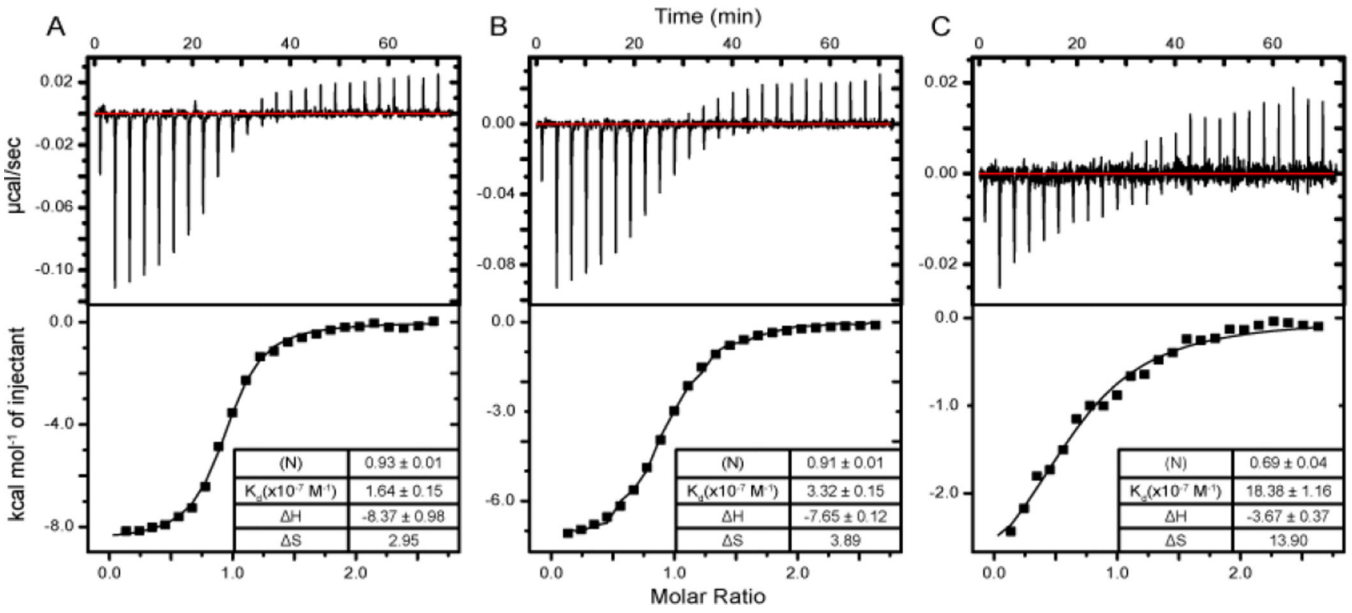

Figure 6. Isothermal titration profiled of Dlx5- (A), Dlx5[Q178P]- (B) and Dlx5[Q186H]-(C) binding to DNA

100 µM proteins solutions were added to a 7.5 µM solution of the 14 bp dsDNA in 20 mM sodium phosphate and 300 mM sodium chloride at pH 6.0 and 20 °C. The top panels show heats observed as a result of 24 injections of the proteins into the DNA solution at 175 second intervals. The bottom panels show binding enthalpies evaluated with the assumption of a one-site binding model.

Table 1

X-ray data collection and refinement statistics (PDB ID 4RDU)

Data collection	
Beamline	SSRL 14-1
Unit cell (Å)	a=34.18, b=42.91, c=56.10 α=84.13°, β=77.33°, γ=67.13°
Spacegroup	P1
Wavelength (Å)	1.000
Resolution range (Å)	22.31-1.85
No. observations	44,904
No. unique reflections	23,348
Completeness (%)	95.5 (94.1)
Mean I/σ (I)	8.0 (2.2)
R_{merge} on I(%)[a]	4.6 (27.1)
R_{meas} on I(%)[b]	6.8 (38.3)
R_{pim} on I(%)[c]	4.6 (27.1)
Highest resolution shell (Å)	1.90-1.85
Model and Refinement Statistics	
Resolution range (Å)	22.31-1.85
No. reflections (total)	23,315[d]
No. reflections (test)	1,188
Cutoff criteria	|F|>0
R_{cryst}(%)[e]	18.5
R_{free} (%)[e]	22.5
Stereochemical Parameters	
Bond lengths (Å)	0.011
Bond angles (°)	1.32
MolProbity Clash Score	0.84
Average isotropic B-value, protein (Å^2)[g]	52.8
Average isotropic B-value, DNA (Å^2)[g]	49.4
Wilson B-value (Å^2)	33.7
ESU based on R_{free} (Å)[h]	0.14
No. protein chains/residues/atoms	2/123/1044
No. nucleic chains/residues/atoms	4/55/1114
No. waters	232
Ramachandran plot (%)[f]	100
Rotamer outliers (%)	0

Values in parentheses are for the highest resolution shell.

[a] $R_{merge} = \Sigma_{hkl}[\Sigma_i|I_i(hkl) - (I(hkl))|/\Sigma_{hkl}\Sigma_i(hkl)$.

[b] $R_{meas} = \Sigma_{hkl}[N/(N-1)]^{1/2}\Sigma_i|I_i(hkl) - (I(hkl))|/\Sigma_{hkl}\Sigma_i I_i(hkl)$ [59].

[c] $R_{p.i.m}$ (precision-indicating R_{merge}) = $\Sigma_{hkl}[(1/(N-1)]^{1/2} \Sigma_i|I_i(hkl) - <I(hkl)>| / \Sigma_{hkl}\Sigma_i I_i(hkl)$ [60, 61].

[d] Typically, the number of unique reflections used in refinement is slightly less than the total number that were integrated and scaled. Reflections are excluded owing to negative intensities and rounding errors in the resolution limits and unit-cell parameters.

[e] $R_{cryst} = \Sigma_{hkl}||F_{obs}| - |F_{calc}||/\Sigma_{hkl}|F_{obs}|$, where F_{calc} and F_{obs} are the calculated and observed structure-factor amplitudes, respectively. R_{free} is the same as R_{cryst} but for 5.0% of the total reflections chosen at random and omitted from refinement.

[f] Percentage of residues in favored regions of Ramachandran plot.

[g] This value represents the total B that includes TLS and residual B components.

[h] Estimated overall coordinate error [62]